

Quantum Monte Carlo Calculation of the Binding Energy of Bilayer Graphene

E. Mostaani, N. D. Drummond, and V. I. Fal'ko

Department of Physics, Lancaster University, Lancaster LA1 4YB, United Kingdom

(Dated: August 23, 2018)

We report diffusion quantum Monte Carlo calculations of the interlayer binding energy of bilayer graphene. We find the binding energies of the AA- and AB-stacked structures at the equilibrium separation to be 11.5(9) and 17.7(9) meV/atom, respectively. The out-of-plane zone-center optical phonon frequency predicted by our binding-energy curve is consistent with available experimental results. As well as assisting the modeling of interactions between graphene layers, our results will facilitate the development of van der Waals exchange–correlation functionals for density functional theory calculations.

PACS numbers: 61.48.Gh, 71.15.Nc, 02.70.Ss

van der Waals (vdW) interactions play a crucial role in a wide range of physical and biological phenomena, from the binding of rare-gas solids to the folding of proteins. Significant efforts are therefore being made to develop computational methods that predict vdW contributions to energies of adhesion, particularly for materials such as multilayer graphene. This task has proved to be challenging, however, because vdW interactions are caused by nonlocal electron correlation effects. Standard first-principles approaches such as density functional theory (DFT) with local exchange–correlation functionals do not describe vdW interactions accurately. One technique for including vdW interactions in a first-principles framework is to add energies obtained using pairwise interatomic potentials to DFT total energies; this is the so-called DFT-D scheme [1–4]. The development of vdW density functionals (vdW-DFs) that can describe vdW interactions in a seamless fashion is another promising approach [5–8]. DFT-based random-phase approximation (RPA) calculations of the correlation energy [9, 10] provide a more sophisticated method for treating vdW interactions; however, RPA atomization energies are typically overestimated by up to 15% for solids [11, 12], and hence the accuracy of this approach is unclear. Symmetry-adapted perturbation theory based on DFT allows one to calculate the vdW interactions between molecules and hence, by extrapolation, between nanostructures [13]. Finally, empirical interatomic potentials with r^{-6} tails may be used to calculate binding energies [14, 15], although such potentials give a qualitatively incorrect description of the interaction of metallic or π -bonded two-dimensional (2D) materials at large separation [16].

A key test system for methods purporting to describe vdW interactions between low-dimensional materials is bilayer graphene (BLG). Several theoretical studies have used methods based on DFT to calculate the binding energy (BE) of BLG. Some of the results are summarized in Table I, but there is very little consensus. In this work we provide diffusion quantum Monte Carlo (DMC) data for the BE of BLG and the atomization

TABLE I: BE of BLG (both AA- and AB-stacked) obtained in recent theoretical studies. The layer separations d quoted in the table are the ones used in the calculations, not necessarily the optimized bond length for the given method. “SAPT(DFT)” and “DFT-LCAO-OO” denote symmetry-adapted perturbation theory based on DFT and linear combination of atomic orbitals-orbital occupancy based on DFT, respectively.

Stacking	Method	d (Å)	BE (meV/atom)
AA	vdW-DF [17]	3.35	10.4
AA	DFT-D [17]	3.25	31.1
AA	DMC (pres. wk.)	3.495	11.5(9)
AB	DFT-LCAO-OO [18]	3.1–3.2	70(5)
AB	SAPT(DFT) [19]	3.43	42.5
AB	vdW-DF [7]	3.6	45.5
AB	vdW-DF [17]	3.35	29.3
AB	DFT-D [17]	3.25	50.6
AB	DFT-D [20]	3.32	22
AB	DMC (pres. wk.)	3.384	17.7(9)

energy of monolayer graphene (MLG), which we have extrapolated to the thermodynamic limit. We find the DMC BE of BLG to be somewhat less than the BEs predicted by DFT-D, although the latter vary significantly from scheme to scheme. The DMC method is the most accurate first-principles technique available for studying condensed matter. Our data can therefore be used as a benchmark for the development of vdW functionals.

We have used the variational quantum Monte Carlo and DMC methods as implemented in the CASINO code [21] to study MLG and BLG. In the former method, Monte Carlo integration is used to evaluate expectation values with respect to trial many-body wave-function forms that may be of arbitrary complexity. In the DMC method [22, 23], a stochastic process governed by the Schrödinger equation in imaginary time is simulated to project out the ground-state component of the trial wave function. Fermionic antisymmetry is maintained by the fixed-node approximation, in which the nodal surface is

constrained to equal that of the trial wave function [24]. DMC methods have recently been used to study the BE of hexagonal boron nitride bilayers [25].

Our many-body trial wave-function form consisted of Slater determinants for spin-up and spin-down electrons multiplied by a symmetric, positive Jastrow correlation factor $\exp(J)$ [23]. The Slater determinants contained Kohn-Sham orbitals that were generated using the CASTEP plane-wave DFT code [26] within the local density approximation (LDA). We performed test DMC calculations for 3×3 supercells of MLG and AB-stacked BLG using Perdew-Burke-Ernzerhof (PBE) [27] orbitals. The effect of changing the orbitals on the DMC total energies (and hence the BE) was statistically insignificant.

To improve the scaling of our DMC calculations and to allow the use of 2D-periodic boundary conditions, the orbitals were re-represented in a B-spline (blip) basis [28]. The Jastrow exponent J consisted of polynomial and plane-wave expansions in the electron-ion and electron-electron distances [29]. The free parameters in the Jastrow factor were optimized by unweighted variance minimization [30, 31]. The DMC energy was extrapolated linearly to zero time step and we verified that finite-population errors in our results are negligible [32]. The fixed-node error is of uncertain magnitude, but it is always positive, and should largely cancel when the BE is calculated. We used Dirac-Fock pseudopotentials to represent the C atoms [33, 34] and fixed the in-plane lattice parameter at the experimental value of $a = 2.460 \text{ \AA}$.

The principal source of uncertainty in our BE results is the need to use finite simulation cells subject to periodic boundary conditions in DMC calculations for condensed matter. Finite-size errors in DMC total energies consist of (i) pseudorandom, oscillatory single-particle finite-size errors due to momentum quantization and (ii) systematic finite-size errors due to the inability to describe long-range two-body correlations and the difference between $1/r$ and the 2D Ewald interaction [35, 36] in a finite periodic cell. By dividing the electron-electron interaction energy into a Hartree term (the electrostatic energy of the charge density) and an exchange-correlation energy (the interaction energy of each electron with its accompanying exchange-correlation hole) and considering the long-range nonoscillatory behavior of the hole predicted by the RPA, it can be shown that the systematic finite-size error in the interaction energy per electron of a 2D-periodic system is negative and scales asymptotically with system size N as $O(N^{-5/4})$ [37]. The leading-order long-range finite-size error in the kinetic energy per electron behaves in a similar fashion. The finite-size error in the atomization energy is therefore positive and scales as $O(N^{-5/4})$, and the finite-size error in the BE per atom must also exhibit the $O(N^{-5/4})$ scaling. We also investigated finite-size errors in the asymptotic BE using the Lifshitz theory of vdW interactions [38, 39] with a Dirac model of electron dispersion in graphene. To study finite

system sizes, we introduced a cutoff wavelength that depended on the cell size and layer separation. However, near the equilibrium separation, short-range interactions are important and the contribution to the finite-size error from the Lifshitz theory is negligible. In order to eliminate finite-size effects and obtain the atomization and binding energies in the thermodynamic limit, we studied simulation cells consisting of arrays of 3×3 , 4×4 , and 6×6 primitive cells for MLG and BLG at the equilibrium layer separation and 3×3 and 5×5 cells for BLG at nonequilibrium layer separations. We used canonical-ensemble twist averaging [40] (i.e., averaging over offsets to the grid of \mathbf{k} vectors) to reduce the oscillatory single-particle finite-size errors in the ground-state energies of MLG and BLG. To obtain the twist-averaged energy of MLG in a simulation cell containing N_P primitive cells, we performed DMC calculations at twelve random offsets \mathbf{k}_s to the grid of \mathbf{k} vectors, then fitted

$$E(N_P, \mathbf{k}_s) = \bar{E}(N_P) + b[E_{\text{LDA}}(N_P, \mathbf{k}_s) - E_{\text{LDA}}(\infty)] \quad (1)$$

to the DMC energies per atom $E(N_P, \mathbf{k}_s)$. The model function has two fitting parameters: $\bar{E}(N_P)$, which is the twist-averaged DMC energy per atom, and b . $E_{\text{LDA}}(N_P, \mathbf{k}_s)$ is the DFT-LDA energy per atom of MLG obtained using the offset \mathbf{k} -point grid corresponding to the supercell used in the DMC calculations, and $E_{\text{LDA}}(\infty)$ is the DFT-LDA energy per atom obtained using a fine (50×50) \mathbf{k} -point mesh. Finally, we extrapolated our total-energy data to infinite system size by fitting

$$\bar{E}(N_P) = E(\infty) + cN_P^{-5/4} \quad (2)$$

to the twist-averaged energies per atom, where the extrapolated energy per atom $E(\infty)$ and c are fitting parameters. The atomization energy of MLG is the difference between the energy of an isolated, spin-polarized C atom and the energy per atom of MLG.

Our DMC atomization energies of MLG as a function of system size are plotted in Fig. 1. We find the static-nucleus DMC atomization energy to be $7.395(3) \text{ eV/atom}$ with a Slater-Jastrow trial wave function. This is lower than the DMC result of $7.464(10) \text{ eV/atom}$ reported in Ref. [41]. Most of this disagreement arises from the use of different pseudopotentials in the two works [32]. The DFT-PBE phonon zero-point energy (ZPE) of MLG was calculated using the method of finite displacements in a 6×6 supercell [42] and found to be 0.165 eV/atom . The ZPE is a correction to be subtracted from the static-nucleus atomization energy. In principle, an accurate first-principles atomization energy for graphene could be used to estimate the BE of graphite by taking the difference of the experimental atomization energy of graphite [$7.371(5) \text{ eV/atom}$ [43]] and the ZPE-corrected atomization energy of MLG. However, the spread of DFT atomization energies resulting from different choices of pseudopotential (of order $40\text{--}70 \text{ meV/atom}$ [32]) implies that

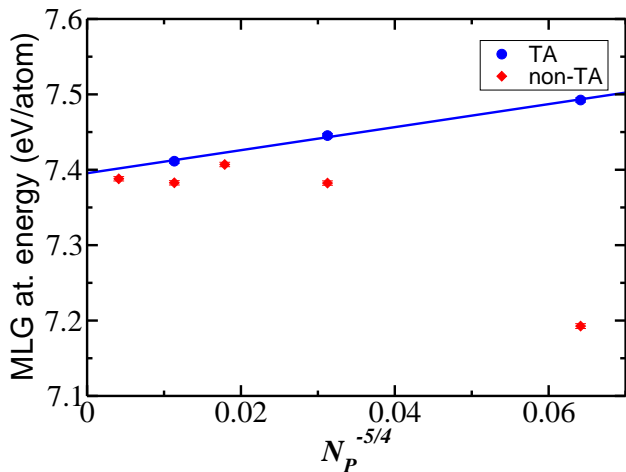


FIG. 1: (Color online) Twist-averaged (TA) and non-TA atomization energies of MLG against $N_P^{-5/4}$ as calculated by DMC, where N_P is the number of primitive cells in the simulation supercell.

first-principles pseudopotential calculations cannot currently be used to calculate the BE of graphite by this approach.

Despite a great deal of theoretical and experimental work, the BE of graphene layers remains poorly understood. The cleavage energy of graphite has been measured to be 43(5) meV/atom [14], the BE to be 35(10) meV/atom [44], and the exfoliation energy to be 52(5) meV/atom [45]. More recent experimental work has found the cleavage energy to be 31(2) meV/atom [46]. It has been suggested that the latter result may be substantially underestimated, because the experimental data were analyzed using a Lennard-Jones potential, which gives qualitatively incorrect interlayer BEs at large separation [47]. Similar difficulties of interpretation may affect the other experimental results in the literature. The results obtained in these works are widely scattered. The DMC method has previously been applied to calculate the BE of graphite [48], which was found to be 56(5) meV/atom, although these calculations were performed in relatively small simulation supercells, and finite-size effects may limit the accuracy of the results obtained.

For BLG, we restrict our attention to the nonretarded regime [49], in which the BE is simply the difference between the nonrelativistic total energy per atom in the monolayer and the bilayer. We used vdW-DF layer separations of $d = 3.495$ Å and 3.384 Å [50] for the AA- and AB-stacked configurations, respectively. In Fig. 2 we plot the twist-averaged BEs of AA- and AB-stacked BLG as a function of system size. Non-twist-averaged BEs are shown in the inset to Fig. 2 and, as expected, show large oscillations due to momentum-quantization effects. For widely separated graphene layers with nonoverlapping charge densities, single-particle finite-size errors cancel

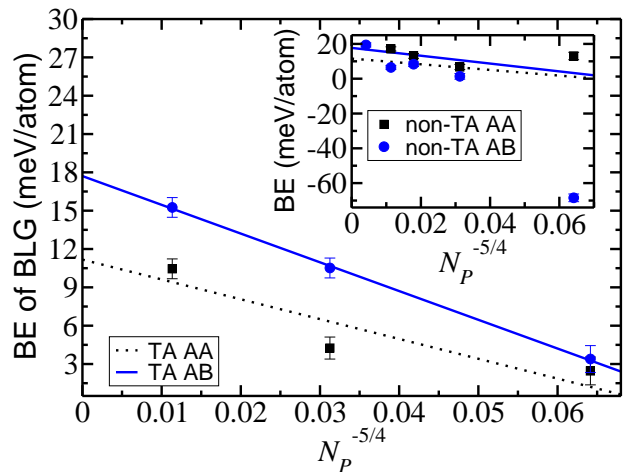


FIG. 2: (Color online) Twist-averaged (TA) BLG BE against $N_P^{-5/4}$ as calculated by DMC, where N_P is the number of primitive cells in the simulation supercell. The inset shows non-twist-averaged BEs. The layer separations are the vdW-DF [50] equilibrium values of 3.495 and 3.384 Å for the AA- and AB-stacked structures, respectively.

perfectly when the BE is calculated. However, when the layers are closer together, the cancellation is no longer perfect. In practice, near the equilibrium separation, the single-particle errors in the BE correlate closely with the single-particle errors in the total energy of BLG. To evaluate the BE in the thermodynamic limit, we twist-averaged the BE using Eq. (1) with the BE per atom in place of $E(N_P, \mathbf{k}_s)$ and the DFT-LDA total energy per atom of BLG in place of $E_{\text{LDA}}(N_P, \mathbf{k}_s)$. We then extrapolated the twist-averaged BE to infinite system size using Eq. (2). As shown in Fig. 2, the BE of AB-stacked BLG is larger than that of AA-stacked BLG, confirming that the former is the more stable structure.

The area of a simulation cell with N_P unit cells is $A = \sqrt{3}N_P a^2/2$, where a is the lattice parameter of graphene. If we define the linear size L of the cell via $\pi L^2 = A$ then we may express the twist-averaged BE per atom as $\bar{E}_{\text{bind}}(L) = E_{\text{bind}}(\infty) + c' L^{-5/2}$, where c' is $-0.31(5)$ and $-0.43(5)$ eV Å^{5/2} for the AA-stacked and AB-stacked geometries, respectively. The BE is reduced at small supercell sizes L . The use of a finite supercell crudely models the situation where the Coulomb interaction between electrons is screened by a metallic substrate. Hence a metallic substrate is expected to weaken the binding of BLG.

In Fig. 3 we plot the BE of AB-stacked BLG against the interlayer separation, as calculated by DFT, DFT-D, and DMC. The layer separations we have studied are not in the asymptotic regime in which the BE falls off as d^{-3} , where d is the interlayer separation [51]. We have fitted the function $E_{\text{bind}}(d) = A_4 d^{-4} + A_8 d^{-8} + A_{12} d^{-12} + A_{16} d^{-16}$ to our DMC BE data, where the $\{A_i\}$ are fitting

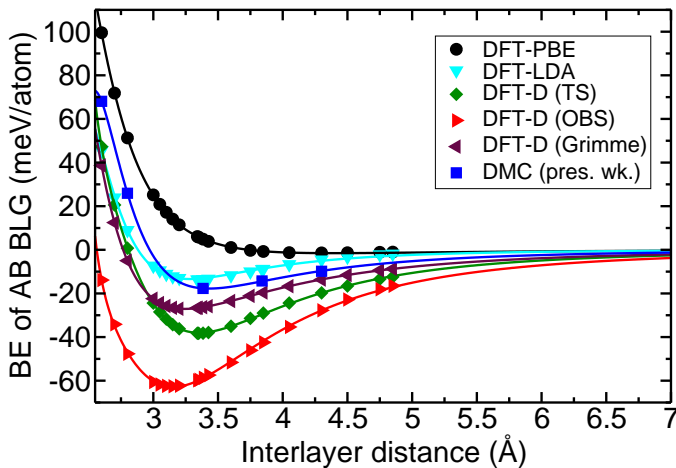


FIG. 3: (Color online) BE curve of AB-stacked BLG as a function of interlayer distance calculated using DFT, DFT-D, and DMC methods. Our DFT-D calculations used the Tkatchenko–Scheffler (TS) [4], Ortman–Bechstedt–Schmidt (OBS) [52], and Grimme [53] vdW corrections.

parameters, which we find to be $A_4 = -2.9 \times 10^3 \text{ meV } \text{Å}^4$, $A_8 = -2.97 \times 10^5 \text{ meV } \text{Å}^8$, $A_{12} = 6.18 \times 10^7 \text{ meV } \text{Å}^{12}$, and $A_{16} = -1.63 \times 10^9 \text{ meV } \text{Å}^{16}$. This function fits the DMC data well, with a χ^2 value of 0.007 per data point. The BE found at the minimum of the fitting curve is 17.8(8) meV/atom at the equilibrium separation of 3.43(4) Å. Although the separation that minimizes our fitted BE curve for AB-stacked BLG is somewhat larger than the separation used in our calculation of the BE reported in Table I, the difference between the BEs is not statistically significant. The Tkatchenko–Scheffler [4] DFT-D scheme shows roughly the same equilibrium separation as DMC, but the magnitude of the BE is substantially larger. In general, the three DFT-D methods studied [4, 52, 53] disagree with each other and with DMC. Indeed, the magnitude of the BE (if not the shape of the BE curve) is best described by the LDA. Our fitted BE curve enables us to calculate the out-of plane zone-center optical phonon frequency $\omega_{ZO'}$ of AB-stacked BLG [54]. A comparison of $\omega_{ZO'}$ frequencies obtained by DFT, DMC, and experiments [55, 56] is shown in Table II. Our DFT-LDA frequency is in reasonable agreement with the result (76.8 cm^{-1}) reported in Ref. [57]. The difference between the $\omega_{ZO'}$ frequency predicted by our fit to our DMC data and the experimental result is negligible [3(7) cm^{-1}] [32].

In summary, we have used the DMC method to determine the BE of BLG. Our approach includes a full, first-principles treatment of vdW interactions. We have found the static-nucleus atomization energy of MLG to be 7.395(3) eV/atom, although the uncertainty in this result due to the use of nonlocal pseudopotentials may be as much as 70 meV/atom [32]. We find the BEs of AA- and AB-stacked BLG near their equilibrium separa-

TABLE II: The equilibrium separation d_0 , static-lattice BE at equilibrium separation, and out-of-plane zone-center optical-phonon frequency $\omega_{ZO'}$ of AB-stacked BLG obtained by DFT, DFT-D, DMC, and experiment. The minimum of the curve fitted to the DMC BE data, which is reported in this table, is in statistical agreement with the DMC BE obtained using a fixed layer separation of 3.384 Å, which is reported in Table I.

Method	d_0 (Å)	BE (meV/at.)	$\omega_{ZO'}$ (cm^{-1})
DFT-PBE	4.40	1.53	16
DFT-LDA	3.28	13.38	84
DFT-D (TS)	3.35	38.03	111
DFT-D (OBS)	3.15	62.70	133
DFT-D (Grimme)	3.25	27.08	95
DMC (pres. wk.)	3.43(4)	17.8(8)	83(7)
Exp. [55]			80(2)
Exp. [56]			89

tions to be 11.5(9) and 17.7(9) meV/atom, respectively. Our results indicate that current DFT-D and vdW-DF methods significantly overbind 2D materials.

We acknowledge financial support from the UK Engineering and Physical Sciences Research Council (EPSRC). This work made use of the facilities of Lancaster University’s High-End Computing facility, N8 HPC provided and funded by the N8 consortium and EPSRC (Grant No. EP/K000225/1), and the ARCHER UK National Supercomputing Service. We acknowledge discussions with Andrea C. Ferrari and Silvia Milana.

-
- [1] S. Grimme, *J. Comput. Chem.* **25**, 1463 (2004); S. Grimme, *J. Comput. Chem.* **27**, 1787 (2006).
 - [2] M. Hasegawa, K. Nishidate, and H. Iyetomi, *Phys. Rev. B* **76**, 115424 (2007).
 - [3] S. Grimme *et al.*, *J. Chem. Phys.* **132**, 154104 (2010).
 - [4] A. Tkatchenko and M. Scheffler, *Phys. Rev. Lett.* **102**, 073005 (2009).
 - [5] H. Rydberg *et al.*, *Phys. Rev. Lett.* **91**, 126402 (2003).
 - [6] M. Dion, H. Rydberg, E. Schroder, D.C. Langreth, and B. I. Lundqvist, *Phys. Rev. Lett.* **92**, 246401 (2004); M. Dion, H. Rydberg, E. Schroder, D.C. Langreth, and B.I. Lundqvist, *Phys. Rev. Lett.* **95**, 109902(E) (2005).
 - [7] S.D. Chakarova-Kack, E. Schroder, B.I. Lundqvist, and D.C. Langreth, *Phys. Rev. Lett.* **96**, 146107 (2006).
 - [8] T. Thonhauser *et al.*, *Phys. Rev. B* **76**, 125112 (2007).
 - [9] S. Lebègue *et al.*, *Phys. Rev. Lett.* **105**, 196401 (2010).
 - [10] T. Olsen and K.S. Thygesen, *Phys. Rev. B* **87**, 075111 (2013).
 - [11] H. Eshuis, J.E. Bates, and F. Furche, *Theor. Chem. Acc.* **131**, 1084 (2012).
 - [12] X. Ren *et al.*, *J. Mater. Sci.* **47**, 7447 (2012).
 - [13] B. Jeziorski, R. Moszynski, and K. Szalewicz, *Chem. Rev.* **94**, 1887 (1994).
 - [14] L.A. Girifalco and R.A. Lad, *J. Chem. Phys.* **25**, 693 (1956).

- [15] L.A. Girifalco, M. Hodak, R.S. Lee, Phys. Rev. B **62**, 13104 (2000).
- [16] J.F. Dobson, A. White, and A. Rubio, Phys. Rev. Lett. **96**, 073201 (2006).
- [17] I.V. Lebedeva *et al.*, Phys. Chem. Chem. Phys. **13**, 5687 (2011).
- [18] Y.J. Dappe *et al.*, J. Phys.: Condens. Matter **24**, 424208 (2012).
- [19] R. Podeszwa, J. Chem. Phys. **132**, 044704 (2010).
- [20] T. Gould, S. Lebègue, and J.F. Dobson, J. Phys.: Condens. Matter **25**, 445010 (2013).
- [21] R.J. Needs *et al.*, J. Phys.: Condens. Matter **22**, 023201 (2010).
- [22] D.M. Ceperley and B.J. Alder, Phys. Rev. Lett. **45**, 566 (1980).
- [23] W.M.C. Foulkes *et al.*, Rev. Mod. Phys. **73**, 33 (2001).
- [24] J.B. Anderson, J. Chem. Phys. **65**, 4121 (1976).
- [25] C.-R. Hsing *et al.*, New J. Phys. **16**, 113015 (2014).
- [26] S.J. Clark *et al.*, Z. Kristallogr. **220**, 567 (2005).
- [27] J.P. Perdew, K. Burke, and M. Ernzerhof, Phys. Rev. Lett. **77**, 3865 (1996).
- [28] D. Alfè and M.J. Gillan, Phys. Rev. B **70**, 161101 (2004).
- [29] N.D. Drummond, M.D. Towler, and R.J. Needs, Phys. Rev. B **70**, 235119 (2004).
- [30] N.D. Drummond and R.J. Needs Phys. Rev. B **72**, 085124 (2005).
- [31] C.J. Umrigar, K.G. Wilson, and J.W. Wilkins, Phys. Rev. Lett. **60**, 1719 (1988).
- [32] Supplementary material.
- [33] J.R. Trail and R.J. Needs, J. Chem. Phys. **122**, 014112 (2005).
- [34] J.R. Trail and R.J. Needs, J. Chem. Phys. **122**, 174109 (2005).
- [35] D.E. Parry, Surf. Sci. **49**, 433 (1975); erratum, Surf. Sci. **54**, 195 (1976).
- [36] B. Wood *et al.*, J. Phys.: Condens. Matter **16**, 891 (2004).
- [37] N.D. Drummond, R.J. Needs, A. Sorouri, and W.M.C. Foulkes, Phys. Rev. B **78**, 125106 (2008).
- [38] G. Gómez-Santos, Phys. Rev. B, **80**, 245424 (2009).
- [39] G.L. Klimchitskaya and V.M. Mostepanenko, Phys. Rev. B, **87**, 075439 (2013).
- [40] C. Lin, F.H. Zong, and D.M. Ceperley, Phys. Rev. E **64**, 016702 (2001).
- [41] H. Shin *et al.*, J. Chem. Phys. **140**, 114702 (2014).
- [42] K. Refson, P.R. Tulip, and S.J. Clark, Phys. Rev. B **73**, 155114 (2006).
- [43] CRC Handbook of Chemistry and Physics 91st Edition, W.M. Haynes, (Ed) CRC Press, Inc., Roca Raton, 2010–2011, p. 5-1.
- [44] L.X. Benedict *et al.*, Chem. Phys. Lett. **286**, 490 (1998).
- [45] R. Zacharia, H. Ulbricht, and T. Hertel, Phys. Rev. B **69**, 155406 (2004).
- [46] Z. Liu *et al.*, Phys. Rev. B **85**, 205418 (2012).
- [47] T. Gould *et al.*, J. Chem. Phys. **139**, 224704 (2014).
- [48] L. Spanu, S. Sorella, and G. Galli, Phys. Rev. Lett. **103**, 196401 (2009).
- [49] At large separations the use of the static Coulomb interaction between electrons in two graphene layers ceases to be valid due to the finite speed of light, resulting in a crossover to a regime in which the attractive forces arise from photon zero-point energy [58].
- [50] I. Brihuega *et al.*, Phys. Rev. Lett. **109**, 196802 (2012).
- [51] J.F. Dobson, T. Gould, and G. Vignale, Phys. Rev. X **4**, 021040 (2014).
- [52] F. Ortman, F. Bechstedt, and W.G. Schmidt, Phys. Rev. B **73**, 205101 (2006).
- [53] S. Grimme, J. Comput. Chem. **27**, 1787, (2006).
- [54] The interlayer BE per atom of BLG can be written as $E_{\text{bind}}(d) = E_0 + \frac{1}{8}m_C\omega_{ZO'}^2(d - d_0)^2 + O(d - d_0)^3$, where E_0 is the BE per atom at the equilibrium separation d_0 , m_C is the mass of a carbon atom, and $\omega_{ZO'}$ is the out-of-plane phonon frequency.
- [55] C.H. Lui and T.F. Heinz, Phys. Rev. B **87**, 121404(R) (2013).
- [56] S. Milana, D. Yoon, M. Ijäs, W. P. Han, P.H. Tan, N.M. Pugno, T. Bjorkman, A. Krashenninnikov, and A.C. Ferrari, Determination of Shear Modulus and Out of Plane Young's Modulus of Layered Materials by Raman spectroscopy, Graphene Week, 2015.
- [57] S.K. Saha, U.V. Waghmare, H.R. Krishnamurthy, and A.K. Sood, Phys. Rev. B **78**, 165421 (2008).
- [58] H.B.G. Casimir and D. Polder, Phys. Rev. **73**, 360 (1948).